Journal of Colloid and Interface Science 686 (2025) 852–863

Contents lists available at ScienceDirect

Journal of Colloid And Interface Science

journal homepage: www.elsevier.com/locate/jcis

Effective charge of high-generation PAMAM dendrimers in the adsorbed state

Matthias B. Engelhardt, Paul Markus, Nicolas Helfricht, Georg Papastavrou *

Physical Chemistry II, University of Bayreuth, Universitaetsstrasse 30 95447 Bayreuth, Germany

HIGHLIGHTS

- Followed dendrimer adsorption and characterized charge on different substrates by streaming potential measurement and AFM.
- Effective charge for single poly(amidoamine) dendrimers on different substrates and as a function of pH by correlation of AFM and electrokinetics.
- The diffuse layer of the collector substrates modulated not only the interdendrimers interactions but also determined the effective charge of the dendrimers.

GRAPHICAL ABSTRACT

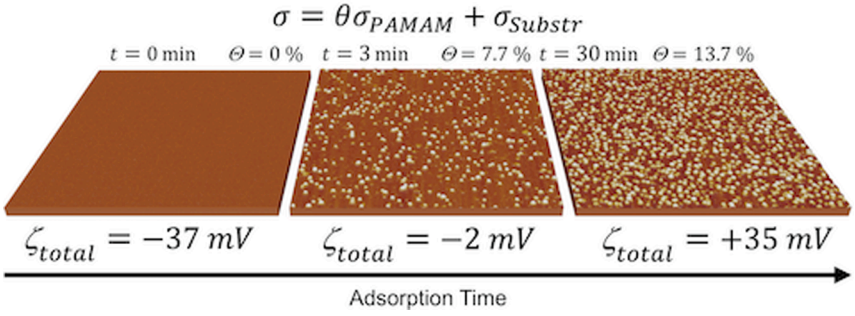

ABSTRACT

The adsorption of macromolecules onto charged surfaces is an ubiquitous process in nature and industrial processes; it has, for example, important implications for surface modification and sensors in analytics. In the case of proteins and some polyelectrolytes, such as dendritic ones, the adsorption process and the resulting final coverage can be described within the framework of the random sequential adsorption (RSA) model. To provide a quantitative description of the intermolecular interaction potential, the effective charge of the molecules is of great importance. The incorporation of charge effects results in the so-called extended or electrostatic RSA model. Here, it is demonstrated for poly(amidoamine) (PAMAM) dendrimers of generation 10 that the influence of the substrate on the effective charge must be considered. Streaming potential measurements of PAMAM G10 adsorbed onto mica and silica showed that the effective charge differed significantly for both substrates. Moreover, for substrates whose surface charge varies with pH, the effective charge varies not only by the titration of the ionizable groups of the polyelectrolytes but also due to the electrostatic interaction with the substrate. A first estimation to account for these effects is provided.

1. Introduction

The adsorption of charged macromolecules to solid substrates is ubiquitous in colloid and interface science [1–5]. Many adsorption processes take place in aqueous solutions, either in natural environment, e.g., the adsorption of humic acid on microplastics [6–8], or for industrial applications, such as the polyelectrolyte-based stabilization of colloidal suspensions or surface modification [5,9–12]. Moreover, many analytical techniques, such as surface plasmon spectroscopy (SPR) or quartz crystal microbalance (QCM), rely on the adsorption of macromolecules, such as proteins, to the sensor [13–16]. Electrolyte/solid interfaces acquire charges, either by protonation/deprotonation of surface functional groups or by ion adsorption [17]. All aforementioned processes have in common that not only the adsorbent, i.e., the macromolecules, but also the collector substrate are charged. Due to the long-range nature of electrostatic forces, the resulting electrostatic interactions play an important role in the adsorption kinetics, as well as in

* Corresponding author.
E-mail address: georg.papastavrou@uni-bayreuth.de (G. Papastavrou).

https://doi.org/10.1016/j.jcis.2025.02.008
Received 12 December 2024; Received in revised form 24 January 2025; Accepted 1 February 2025
Available online 2 February 2025

Nomenclature

List of symbols

a	particle radius for mean-field theory
a_{sol}	radius of a PAMAM dendrimer in solution
a_{ads}	radius of a PAMAM dendrimer in the adsorbed state
a_{eff}	effective radius of a PAMAM dendrimer including interaction potential
A_{PAMAM}	area occupied by one PAMAM dendrimer
C_s	Stern layer capacitance
I	ionic strength
K_L	bulk conductivity of the liquid
k_B	Boltzmann constant
L_B	Bjerrum length
N_A	Avogadrós number
t	adsorption time
T	temperature
U_{str}	streaming potential
Z_{eff}	effective charge in elementary charges
$\widetilde{Z}_{eff}$	normalized effective charge
Z_{ref}	effective charge in reference to published data
Δp	pressure difference
Δx	shift of the shear plane
ε_0	permittivity of free space
ε_r	relative permittivity of the continuum phase
η	dynamic viscosity
κ	inverse Debye length
κ_{eff}	inverse effective Debye length
θ	fractional surface coverage
θ_{jam}	surface coverage in the jamming limit
θ_{plat}	maximum surface coverage in adsorption plateau
ζ	zeta-potential
ζ_{Avg}	zeta-potential measured in an asymmetric cell
ζ_{Ref}	zeta-potential of the reference material
ζ_{Test}	zeta-potential for the substrate under evaluation
σ	total electrokinetic surface charge density
σ_0^{PAMAM}	electrokinetic surface charge density of adsorbed PAMAM dendrimers
σ_0^{sub}	electrokinetic surface charge density of substrate
ψ_d	diffuse layer potential at substrate

reaching a plateau for the maximum adsorbed mass.

The adsorption of polyelectrolytes has been studied extensively in recent decades, including the influence of various parameters such as the polymer topology (e.g. branched versus linear), the charge density, and the molecular weight [2,5,12,18,19]. Dendritic polyelectrolytes play a special role due to their highly-defined shape and low polydispersity index [20–22]. In general, dendrimers can be regarded as nearly comparable to proteins in terms of their adsorption behavior, which can be described within the framework of the random sequential adsorption (RSA) model [23–26]. In particular, poly(amidoamine) (PAMAM) dendrimers have been utilized as model systems for macromolecule adsorption [27,28]. The classical RSA model assumes an ideal collector surface and only hard sphere repulsion between the adsorbing colloids or macromolecules, in particular proteins [25,29,30]. Adamczyk and coworkers have extended this classical RSA model to include the electrostatic repulsion between the adsorbates [23,31]. More recently, also the influence of the substrate has been studied, allowing for a more accurate description of highly charged macromolecular systems [32,33]. We will refer to this approach as the 3-body RSA model.

Electrokinetic methods are often used to characterize charged particles and interfaces in electrolyte solutions [34,35]. Electrophoretic mobility provides information about the charging state of dispersed colloidal objects, including macromolecules, by measuring their mobility in an externally applied electric field [36,37]. Also, PAMAM dendrimers of higher generations have been studied by electrophoretic mobility [38]. For extended flat substrates, the streaming potential technique provides analogous information [34,35]. In this case, the charged macroscopic object, e.g., a silica wafer or a piece of mica, remains stationary and the electrolyte solution is streamed over it, which leads to a displacement of ions in the diffuse layer. The thereby resulting potential difference between two electrodes placed in the channel can be measured and is directly related to the diffuse layer potential of the substrate at the shear plane, the so-called zeta-potential ζ [35]. The streaming potential technique has been applied to bare surfaces and those modified by adsorbed colloids, polymers, and proteins, respectively [27,38–43]. However, the description of determined ζ for heterogeneous charge distributions is often based on a number of assumptions, such as that the charge density of the polyelectrolytes does not depend on the coverage and that it is independent of the state of the collector surface [38,44–46]. Recent studies, including PAMAM dendrimers, indicate that these assumptions are not necessarily fulfilled under all conditions [38,47–50]. Moreover, theoretical studies indicate that the interaction of PAMAM dendrimers with solid substrates is rather complex and includes also conformational changes [51–53].

Here, we study the development of the effective charge of adsorbed PAMAM G10 dendrimers as a function of the surface coverage on different types of substrates *via* streaming potential measurements. The measurements were performed using a custom-made setup developed in our laboratory. By using PAMAM dendrimers of generation 10, we were able to determine the surface coverage by atomic force microscopy (AFM) imaging. The measured streaming potential correlated with the surface coverage, thereby allowing for an unambiguous determination of the effective charge for single dendrimers. This effective charge depended on the substrate, which was unexpected. Moreover, the determined effective charges were different from those calculated on the basis of the mean-field approach [54], which has been previously used to calculate the effective radii in the extended RSA models and the three-body RSA model [28,32,33,55]. This finding has been corroborated by streaming potential measurements as a function of the solution pH on samples with different surface coverage of G10 PAMAM dendrimers. Both the dendrimers and the substrate showed dissociation of functional groups, which led to complex charge regulation of the dendrimers with the substrate. Our experimental results indicate that the effective charge of dendrimers critically depends on the state of the underlying substrate. This finding has important consequences for modeling the 3-body RSA adsorption model and macromolecule adsorption in general.

2. Materials and methods

2.1. Materials

Water of Millipore-quality (MilliQ® IQ 7000, Merck KGaA, Darmstadt, Germany) was used for all preparations and cleaning processes. The specific resistivity of water was 18.2 MΩ cm and the total organic content was always < 6 ppb. Analytic grade potassium chloride (Bio-Ultra, Merck KGaA, Darmstadt, Germany), potassium hydroxide, and hydrochloric acid Titrisol® ampoules (Merck KGaA, Darmstadt, Germany) were used to prepare electrolyte solutions. PAMAM dendrimers of generation 10 were purchased from Dendritech Inc. (Midland, MI, USA). For the collector substrates, muscovite mica (V1-grade, Ted Pella Inc., Redding, CA, USA) and diced fused silica wafer pieces (JGS1-grade, MicroChemicals GmbH, Ulm, Germany) were used.

2.2. Methods

Streaming Potential Setup. Fig. 1 schematically shows the in-house built streaming potential setup. All materials in contact with electrolyte solutions during the measurements were made of glass or fluorinated polymers. A proportional valve (PRA00-A500, AirCom Pneumatic GmbH, Ratingen, Germany) and a 3/2-way valve (Christian Bürkert GmbH & Co. KG, Ingelfingen, Germany) controlled the nitrogen gas stream toward the glass bottles, which were acting as electrolyte reservoirs. Consequently, the electrolyte flow and its direction were controlled by the nitrogen pressure difference between the reservoirs. The electrolyte was driven through the measurement cell. A differential pressure sensor (PX26-005DV, Omega Engineering Inc., Connecticut, USA) was connected to the measurement cell to measure the differential pressure. Cylindrical in-house-built Ag/AgCl electrodes (99.99 % Ag tubes, Advent Research Materials, Oxford, England) were located on both sides of the measurement cell. The electrodes had an inner diameter of 0.8 cm and a length of 5.0 cm. Chlorination of the electrodes was carried out with an electrochemical workstation (Zennium, Zahner-Elektrik GmbH, Kronach, Germany) at a current density of 1 mA cm^{-2} in a 1 M KCl solution for 1 min. The potential difference between the electrodes was determined using an electrometer (Keithley 6514, Tektronix Inc., Oregon, USA). A balance (AND EK-2000i, A&D Company Ltd., Tokyo, Japan) was used to quantify the volume flow rate through the measurement cell. The resulting flow rate was validated using a commercial flow meter (DFM-ECTFE, B.I.O.-TECH e. K., Vilshofen, Germany), which is located between one reservoir and the measurement cell. Furthermore, the measurement setup was equipped with a conductometry cell (3446 conductometry cell, YSI Inc., Ohio, USA) and a Fisherbrand™ pH electrode (Bioblock, Fisher Scientific GmbH, Schwerte, Germany) with an integrated PT100 temperature sensor, which allowed for determining the conductance and temperature in-line between the reservoirs. Therefore, a LCR bridge (HM8118, Rohde & Schwarz GmbH & Co. KG, Munich, Germany) was used to measure the solution conductance in a conductometry cell. All electrical components (proportional valves, pressure sensors, balance, LCR bridge, pH electrode, temperature sensor, flow sensor, and electrometer) were connected to a multifunction I/O device 6008 (National Instruments Corp., Austin, Texas, United States), which allowed interfacing with the software. All components were controlled, and measurement data were collected using a home-written script in IgorPro (version 6.37, Wavemetrics, Portland, OR, USA). The solution pH value was measured using a pH station (827 pH lab, Deutsche Metrohm GmbH & Co. KG, Filderstadt, Germany) and a pH electrode (Aquatrode plus, Deutsche Metrohm GmbH & Co. KG, Filderstadt, Germany) externally before the streaming potential measurements. The asymmetric streaming potential cell was manufactured from non-reinforced poly(tetrafluoroethylene) (PTFE) (Auer Kunststofftechnik GmbH, Olching, Germany). Details of the construction of this cell can be found in the supporting information (SI) (cf. Fig. S1, Table TS1, and Fig. S2). Glass-fiber-reinforced PTFE (ENFLON®, Enflo Canada Ltd., Grand Falls, NB, Canada) was used to build the symmetric streaming potential cell. Further details are given in the SI (cf. Fig. S3, Table TS2, and Figs. S4, S5).

Cleaning of substrates. Adhesive tape was used to cleave the top layer of mica sheets to create molecularly flat pristine interfaces [56]. A modified cleaning procedure from RCA laboratories was used to clean the fused silica wafers [57]. Hellmanex® III surfactant (Hellma Analytics, Müllheim, Germany) solution with a volume fraction of 2 % in water was used to immerse the wafers. The wafers were sonicated for 20 min at 40 °C and then rinsed with water. Next, the samples were immersed in a solution of analytic-grade isopropyl alcohol with a volume fraction of 75 % (VWR Chemical, Darmstadt, Germany) in water and subjected to sonication treatment for 20 min, followed by rinsing with water. Finally, oxidative surface cleaning was performed using a volumetric mixture of laboratory-grade hydrogen peroxide (Fisher Scientific GmbH, Schwerte, Germany), ammonia (25 % in water, AnalaR NORMAPUR®, VWR Chemical), and water at a ratio of 1:1:5. The samples were rinsed with water and dried under a nitrogen stream. The modified RCA treatment was also applied to clean all fluorinated parts of the streaming potential measurement setup in contact with the electrolyte solution.

Dendrimer adsorption. Freshly cleaned substrates were immersed for 0.5–81 min to achieve different fractional surface coverages in a suspension of 5 ppm PAMAM G10 dendrimers at pH = 5 and an overall ionic strength of 5 mM in KCl. Afterward, the substrates were rinsed with approx. 10 mL of water on each side and dried under a nitrogen stream.

Streaming potential measurements. Prior to the measurements, the mounted dry substrates were subjected to 5 min of liquid flow in alternating directions to wet the interface and remove air bubbles from the channel. The electric conductivity of the solution and temperature were recorded for 10 and 100 data points, respectively, and averaged before each streaming potential experiment. In general, a pH titration

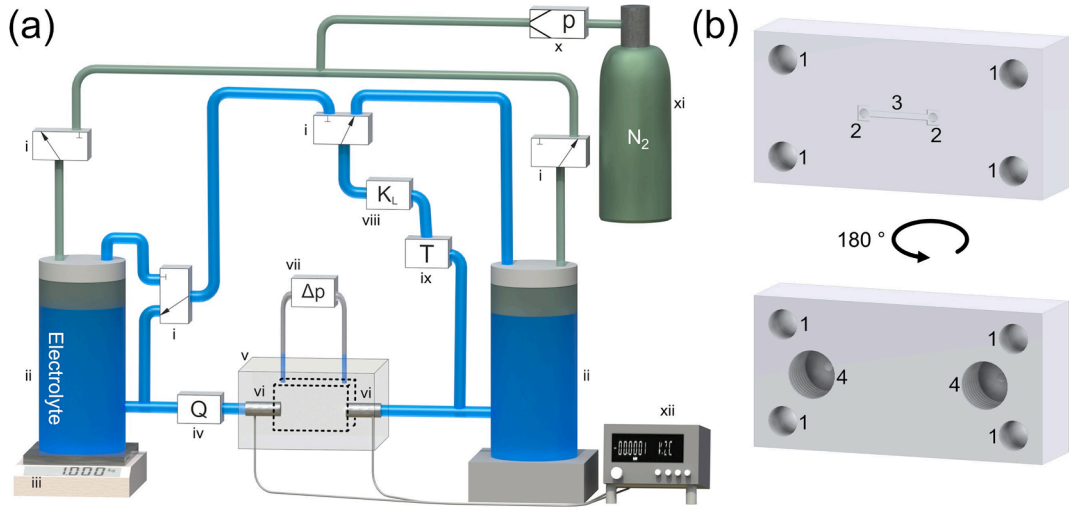

Fig. 1. (a) Schematic illustration of the purposely constructed streaming potential setup with (i) 3/2 way valves, (ii) electrolyte solution reservoirs, (iii) mass flow balance, (iv) flow meter, (v) modular streaming potential cells, (vi) cylindrical Ag/AgCl electrodes, (vii) differential pressure sensor, (viii) conductivity cell, (ix) PT100 temperature sensor, (x) proportional valve, (xi) nitrogen reservoir, and (xii) electrometer. (b) Bottom and top side view of the asymmetric streaming potential cell with (1) mounting holes to connect the cell with the substrate and carrier plate, (2) ends of the tubes that connect the microchannel (3) with the electrodes and electrolyte reservoirs, and (4) threads to connect the cell to the rest of the setup.

was conducted from neutral to either alkaline or acidic pH. For measurements at pH 5, distinct solutions were prepared externally. The experiments recorded the streaming potential and the pressure 10 times at a given applied pressure between ± 200 mbar for 10 different pressures in two directions. The streaming potential coupling coefficient was determined by linear regression of the streaming potential as a function of the applied pressure. The zeta-potential ζ was then calculated using the Helmholtz-Smoluchowski equation for data recorded in the symmetric or asymmetric cell with a PTFE piece as reference substrate. Streaming potential measurements with the asymmetric cell required reference data to evaluate the actual ζ for the test substrates: The procedure outlined by Walker and coworkers was used [58]. The reference data were measured at the pH and ionic strength of interest using the same material as the cell body. The resulting reference curves are shown in the SI (cf. Fig. S6). All streaming potential experiments were conducted at constant ionic strength of 5 mM in KCl between pH 4 and pH 10, or at varying ionic strengths and at a fixed pH of 5.

Atomic Force Microscopy. A Dimension Icon (Bruker Corp., Billerica, MA, USA) equipped with a NanoScope V controller (Bruker Corp., Billerica, MA, USA) was employed in PeakForce Tapping® mode. ScanAsyst Air cantilevers (Bruker Corp., Billerica, MA, USA) were used under ambient conditions to determine the surface topography of pristine and dendrimer-covered substrates. The cantilevers have a nominal resonance frequency of 70 kHz, a nominal spring constant of 0.4 N/m, and a typical tip radius of less than 5 nm. AFM images with scan sizes of (1 × 1) μm^2 were acquired at a scan rate of 0.5 Hz to determine the number density of adsorbed PAMAM dendrimers. The AFM images were evaluated using the NanoScope Analysis software (Version 1.8, Bruker Corp., Billerica, MA, USA). Plane fits of 1st order were applied before counting the number of adsorbed dendrimers.

AFM image evaluation. The number density of PAMAM dendrimers on the inorganic surface was evaluated from at least five flattened AFM images per adsorption state using the Fiji software version 1.54f [59]. We used the "Analyze Particle" function and restricted the particle area to (140 – 1050) nm^2 and circularity between 0.7 and 1. The surface coverage was calculated from the number of adsorbed dendrimers in a 1 μm x 1 μm area and a nominal adsorbed dendrimer radius of 9.15 nm [28]. This procedure was validated with the "Cell Counter" plugin and manual number density determinations (cf. Table S3, Fig. S7, and Table S4, respectively, in the SI).

3. Results and Discussion

3.1. Streaming potential measurements

For this study, we used a purpose-constructed streaming potential setup based on a micro-slit channel configuration with a parallel-plate streaming cell. Our setup was inspired by similar setups from Van Wagenen [60], Werner et al.[61], and Zembala et al.[62,63]. Fig. 1a shows a schematic representation of this streaming potential setup. An external pneumatic pressure was applied to two reservoirs containing electrolyte solution in order to pump the liquid through the measurement cell (cf. Fig. 1b). The pneumatic pressure control was based on a semi-closed system (cf. green lines in Fig. 1a), controlled by a pressure controller for the gas supply lines, and connected to the gas phase of the two liquid reservoirs. The parallel-plate cell (cf. Fig. 1b) was attached in a flow-through configuration to both reservoirs. The hydrostatic pressure difference between the inlet and outlet of the measurement cell was directly measured by a bridging sensor and controlled via a proportional gas valve. The liquid flow through the cell was determined by the mass change in the reservoir using a balance. Determining the liquid volume passing through the cell is essential to verify that a laminar flow regime has been established. Two hollow cylindrical electrodes through which the electrolyte passed were connected to an electrometer to determine the resulting streaming potential U_{str} as a function of the pressure difference Δp.

An electrical double layer of ions is formed at the solid–liquid interface of charged surfaces. The mobile ions in the diffuse layer, i.e., those beyond the plane of the shear, are forced to delocalize from their equilibrium distance when an external pressure is applied and liquid streams along the solid surface [34,35]. The resulting ion delocalization leads to a shift of charges compared to equilibrium without external liquid flow. Consequently, ion movement occurs. This ion movement by the liquid flow accumulates charges at the end of the channel under open-circuit conditions. Thus, a potential builds up for a given pressure difference Δp, which is the streaming potential U_{str}. The current and potential due to the liquid streaming through the channel can be directly measured if two electrodes are placed at both ends of the measurement cell. The relation between ζ and U_{str} is given by the Helmholtz-Smoluchowski approximation [34]:

$$\zeta = \frac{\eta K_L}{\varepsilon_r \varepsilon_0} \frac{U_{str}}{\Delta p} \tag{1}$$

where η is the dynamic viscosity, K_L is the bulk conductivity of the liquid, ε_r is the relative permittivity of the continuum phase, and ε_0 is the permittivity of free space. Equation (1) is based on a two-dimensional flow and a fully developed laminar flow regime in a rectangular channel with a corresponding aspect ratio. In addition, the channel is composed of two chemically identical surfaces. To account for asymmetric electrode potentials, the flow was also reversed for each pressure [64], and discrete pressure ramps were applied to perform a linear regression for eq. (1) [65].

ζ can be also derived for planar-flow cells with two chemically different surfaces [58]. Walker et al. proposed a relation between the measured asymmetric zeta-potential ζ_{Avg}, the zeta-potential of the reference material ζ_{Ref}, and the zeta-potential for the substrate under evaluation ζ_{Test}, respectively:

$$\zeta_{Test} = 2\zeta_{Avg} - \zeta_{Ref} \tag{2}$$

In order to apply eq. (2), ζ_{Ref} has to be determined beforehand in a symmetric cell configuration according to eq. (1). Here, we used PTFE as a reference material for the asymmetric planar-flow cell, which is shown in Fig. 1b.

The electrokinetic charge density σ in the diffuse layer can be calculated from ζ by the modified Grahame equation according to Ohshima [66]:

$$\sigma = \frac{2\varepsilon_r \varepsilon_0 k_B T}{e} \kappa sinh\left(\frac{e\zeta}{2k_B T}\right) \tag{3}$$

κ^{-1} is the so-called Debye length, which is given for a 1:1 electrolyte as [17]:

$$\kappa^{-1} = \sqrt{\frac{\varepsilon_r \varepsilon_0 k_B T}{2N_A I e^2}} \tag{4}$$

Here, k_B is the Boltzmann constant, T is the temperature, N_A is Avogadrós number, I is the ionic strength in mol m^{-3}, and e is the elementary charge.

3.2. Characterization of the substrates

In this study, we concentrated on two different collector surfaces for the adsorption of PAMAM dendrimers: fused silica and muscovite mica. Both substrates have been previously studied by streaming potential measurements, albeit under slightly different electrolyte conditions [67–69]. Moreover, there is a significant scattering in the literature for the streaming potentials of these two surfaces. Muscovite mica is a natural material [70], hence its properties vary with origin. In addition, the time between preparation and measurement plays an important role [71,72]. Moreover, the release of potassium ions and adsorption of

electrolyte ions to mica account for variations in the reported ζ [72]. Also, in the case of silica, the preparation history is of crucial importance for the electrokinetic properties [73]. All data presented in the following have been acquired with an asymmetric measurement cell. In the case of mica, we also performed a comparison for a symmetric planar-flow cell. The corresponding data are provided in the supporting information (cf. Fig. S8).

Fig. 2a shows ζ of mica as a function of pH for two ionic strengths (1 mM and 5 mM, respectively). The ionic strength of 1 mM is shown only for comparison with the literature values. The here-determined ζ match the values reported previously [67–69]. No significant dependence of ζ on pH has been observed for both ionic strengths, which is in-line with literature [68,74].

Fig. 2b shows ζ as function of pH for fused silica substrates under analogous conditions to mica substrates. The silica wafers have always been freshly oxidized by a modified RCA-procedure [57]. As expected for silica surfaces, a clear dependence of ζ on the pH has been observed [76,77]. The here acquired data at $I = 5$ mM fall between the data reported for $I = 1$ mM and 10 mM [75]. Moreover, the main characteristics of the 1-pK model proposed for silica have been reproduced [73,76–78]. The solid red line in Fig. 2b is based on a total site density of silanol groups $\Gamma = 5{\cdot}10^8$ m^{-2} and a pK$_a$ of 5.8, similar to values reported previously [75]. ζ(pH) has been calculated from ψ_d(pH) by

$$\zeta = \frac{4}{k_B T e} arctanh\left[\exp(-\kappa\Delta x) tanh\left(\frac{k_B T e \psi_d}{4}\right)\right] \quad (5)$$

for large κh analogously to Kobayashi et al.[79] where h corresponds to the channel height. For the calculation, we assume a Stern layer capacitance $C_s = 1.4$ F m^{-2} (cf. ref. [75]) and a shift of the shear plane by $\Delta x = 1.5$ nm due to the surface roughness (cf. Fig. S9) of the fused silica substrate [78].

The surface charge densities σ of the substrates are important for the following data analysis and can be calculated using the modified Grahame equation (cf. Eq. (3)) from the here-obtained ζ. In order to verify the validity of Eq. (3) for our purposes, we additionally determined ζ as a function of the ionic strength I for constant pH = 5. Fig. 3 shows the corresponding data for muscovite mica (cf. Fig. 3a) and fused silica (cf. Fig. 3b). Data for mica acquired in a symmetric streaming potential cell are compiled in the SI (cf. Fig. S10) and fall in the same range of values as those obtained with the asymmetric cell. The solid lines indicate the fits to Eq. (3) and provide an estimate of the electrokinetic charge density σ of both substrates. We find σ = -6.9 ± 0.2 mC m^{-2} for muscovite mica and -8.4 ± 0.4 mC m^{-2} for fused silica. The latter value for the silica substrate is in good agreement with values calculated from the literature under nearly comparable conditions with -8.3 ± 1.9 mC m^{-2} by Scales et al. and -8.1 ± 1.1 mC m^{-2} by Kosior et al., respectively [67,80]. The lower charge density of the mica substrate can be rationalized in terms of ion adsorption [81]. Nevertheless, the charge density for mica was lower than reported elsewhere, albeit measured at higher pH [67,82]. However, also smaller values have been reported from Israelachvili and Adams [83]. Lyons and coworkers [74] found no dependence for mica of ζ on pH with low ζ-values, using the mica as the aforementioned study. Hence, there might be a relationship between low charge densities and no obvious pH dependence.

3.3. Adsorption of PAMAM dendrimers

PAMAM dendrimers are monodisperse macromolecules, which have an onion-like structure and a spherical shape in solution (cf. Fig. 4a) [20,84]. For PAMAM G10 a radius $a_{sol} = 6.75$ nm in solution has been reported [28]. However, upon adsorption onto a solid substrate, the dendrimers deform (cf. schematic representation in Fig. 4b) as demonstrated by simulations [51–53], and corroborated by AFM imaging [22,22,28,85–88]. When adsorbed to mica, their radius increases while flattening leads to a reduced height. Here, we assume $a_{ads} = 9.15$ nm and a height of 4.28 nm [28]. Recent studies indicate that the dimensions in the adsorbed state depend on the electrolyte, pH, ionic strength, and type of substrate [49,50]. A PAMAM G10 dendrimer has 4096 ionizable groups, which are practically all charged at pH 4–5 [89]. However, the condensation of counter ions does lead to a strongly reduced effective charge Z_{eff} compared to the bare charge. For Z_{eff}, Bocquet et al. approximated the limit of low ionic strength and large particle radii a [54]:

$$Z_{eff} = \frac{a}{L_B}(4\kappa a + 6) \quad (6)$$

where L_B is the Bjerrum length and a is the radius. This Z_{eff} is responsible for the interdendrimer or interparticle repulsion in the extended (or electrostatic) RSA model and leads in the framework of the RSA model to an increased, effective radius that critically depends on the total ionic strength [4,31].

The adsorption kinetics and the resulting saturated layer of adsorbed PAMAM dendrimers has been studied previously [28,32,33,38,47,48,90]. PAMAM adsorption can be followed by atomic force microscopy (AFM) [28,32], quartz crystal microbalance (QCM) [47], streaming potential [38], and reflectometry [33,90]. The

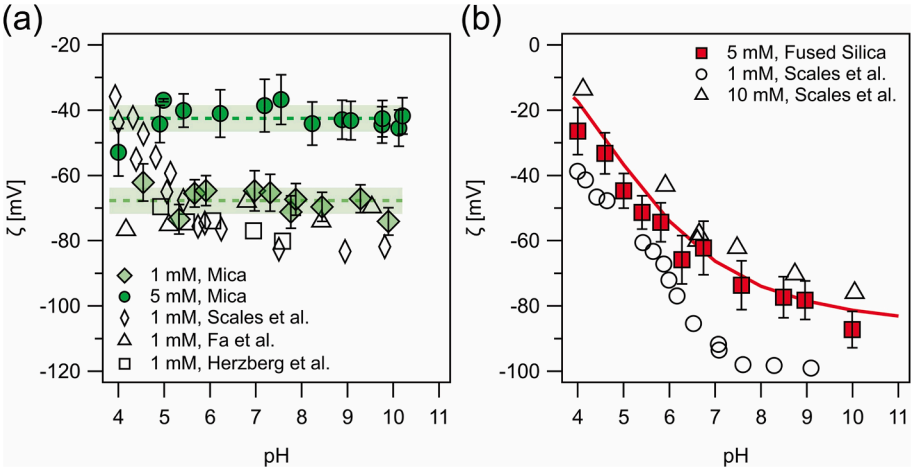

Fig. 2. Zeta-potential ζ of (a) muscovite mica and (b) fused silica as functions of pH (filled data points) in KCl. The pH titrations of mica were carried out at ionic strengths of 1 mM and 5 mM, whereas silica was studied only at 5 mM. All data presented have been acquired using an asymmetric cell. For comparison, data reported in the literature are shown (open data points) [67–69,75]. The dashed lines are the mean constant ζ with the corresponding standard deviations for ζ for mica at 1 mM and 5 mM ionic strength, respectively, in (a), while the solid line represents the 1-pK model used to describe the pH dependence of silica (b).

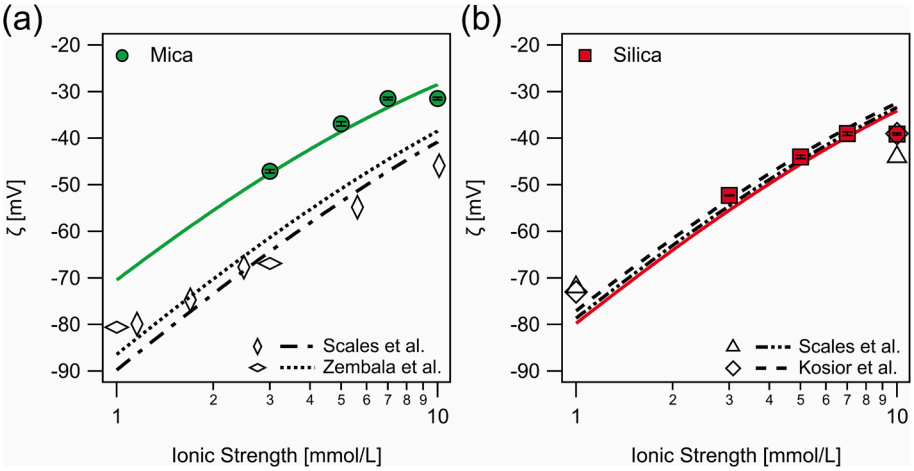

Fig. 3. Zeta-potential ζ of muscovite mica (a) and fused silica (b) as function of the ionic strength at pH = 5. Open symbols show literature data acquired at pH 5.8 [67,75,80,82]. Fits to the modified Grahame equation of the presented data are shown as solid lines. The broken and dashed lines originate from fits to the literature data.

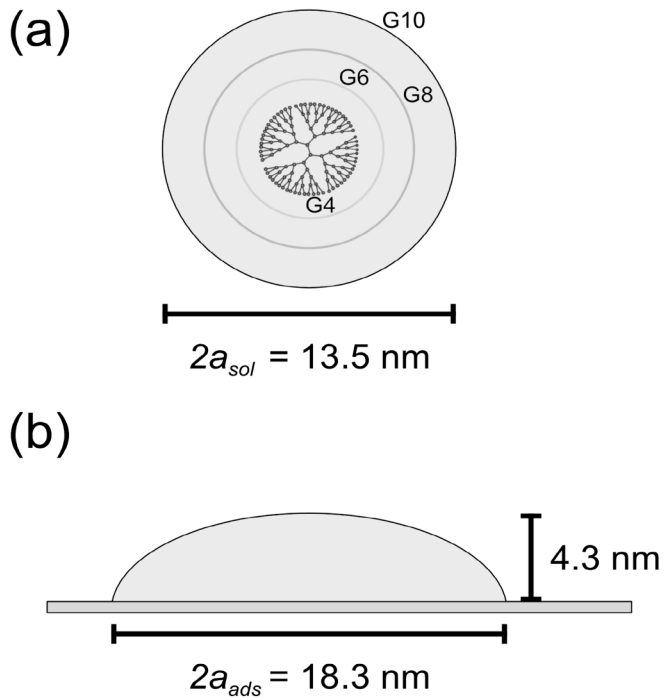

Fig. 4. (a) Schematic representation of poly(amidoamine) (PAMAM) dendrimers of generation 10 in solution. The different generations grow in an onion-like structure during polymerization. PAMAM G10 has a solution radius a_{sol}. Modified from Pericet-Camara et al. [32] (b) Upon adsorption, the dendrimers flatten with a larger radius a_{ads} [28]. The geometrical dimensions used in this study are shown.

adsorption of PAMAM G10 dendrimers can be qualitatively described within the framework of the electrostatic random sequential (RSA) model [28]. Due to the repulsion between the dendrimers based on the overlap of their electrical double layers, the surface coverage depends on the electrostatic screening and thus the electrolyte's ionic strength. However, the charge of the collector surface creates a double layer. This affects the screening length and changes the interdendrimer interaction potential as described by the 3-body RSA model [32,33].

Fig. 5 shows AFM images of substrates with PAMAM G10 adsorbed on mica and silica substrates. The images were acquired in air using PeakForce Tapping® mode. As expected, different fractional surface coverages were obtained depending on the adsorption time. For adsorption times greater than 15 min, an adsorption plateau was reached for both types of surfaces. Due to the repulsive interaction between the like-charged dendrimers, there remains a minimal distance between the adsorbed dendrimers, as predicted by the extended RSA model. Moreover, the substrate has an influence according to the 3-body RSA model [32,33]. The previously reported lower coverage on silica than for mica has also been observed here [32]. However, it should be noted that the effect was less pronounced as the adsorption was carried out at a higher ionic strength compared to the aforementioned study. The number of adsorbed dendrimers was determined by automatic image analysis from at least five AFM images acquired at different spots on the substrates. To convert dendrimer number densities to fractional surface coverage θ, we used previously reported dimensions of adsorbed PAMAM G10 dendrimers of a_{ads} = 9.15 nm [28]. It should be stressed that a quantitative description of the adsorption kinetics is not necessary for the here-conducted experiments, as the surface coverage can be determined independently by AFM imaging for each adsorption time.

3.4. Fractional surface coverage and zeta-potential ζ

Fig. 6 plots the surface coverage θ as function of adsorption time t. A linear dependence $\theta(t) \propto \sqrt{t}$ has been observed as long as the so-called jamming limit has not been reached, which is in-line with a diffusion limited transport [24,28,33]. This dependence $\propto \sqrt{t}$ has been observed for the initial adsorption onto both substrates (cf. Fig. 6a,b). The similar slopes for mica (cf. Fig. 6a) and silica (cf. Fig. 6b) indicate that the sticking coefficients for both surfaces were approximately comparable. For both materials, the surface coverage reached a plateau for $t \gtrsim 15$ min. These findings were also verified for mica in a symmetric streaming potential cell (cf. Fig. S12 and the corresponding data in Fig. S11). The existence of plateaus with $\theta < 1$ in coverage was expected within the framework of the RSA model and corresponded to the jamming limit θ_{jam} based on the effective radius of the PAMAM G10 dendrimers due to their electrostatic interaction. However, the plateaus differed significantly for these two substrates, which has already been observed previously [32]. On fused silica, a surface coverage of about $\theta_{plat} = 0.092 \pm 0.002$ has been determined. By contrast, we found about $\theta_{plat} = 0.135 \pm 0.003$ for mica. We compared the experimental values to the theoretical values for θ_{plat} calculated on the basis of the extended RSA model, considering Z_{eff} based on the mean-field approach according to Eq. (6). We found a clear deviation from the experimental values. We return to this point at a later stage when Z_{eff} will be determined independently by the streaming potential measurements presented in the following.

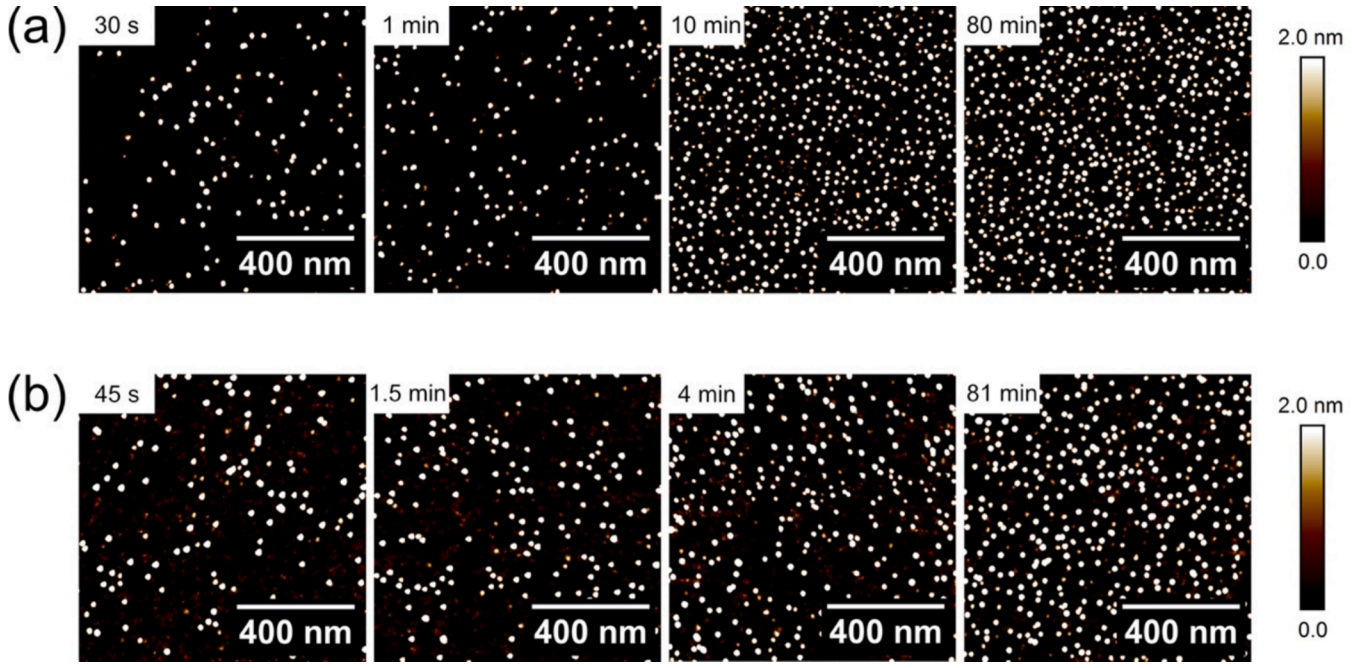

Fig. 5. AFM images of PAMAM G10 dendrimers adsorbed on (a) mica and (b) silica surfaces for different adsorption times. The scan size was always 1 μm x 1 μm and the images were acquired in air using PeakForce Tapping® mode. Slight variations in the dimensions of the dendrimers were attributed to the different AFM tips used.

Fig. 6c,d show ζ as function of the adsorption time t determined according to equations (1) and (2). The fractional surface coverage was characterized by AFM for a simultaneously prepared sample. For both surfaces, the values of $\zeta(t)$ correlate strongly with coverage $\theta(t)$. This correlation is elucidated in the following paragraph in more detail as it allows to estimate Z_{eff}.

3.5. Determination of effective charge in the adsorbed state

Fig. 7a shows ζ as a function of the fractional surface coverage θ. For both substrates ζ was increasing quasi-linearly with surface coverage. However, the slope of this increase is significantly different and is related to a different Z_{eff} on both substrates: Assuming that each PAMAM G10 dendrimer carries an effective charge Z_{eff} and occupies an area $A_{PAMAM} = \pi a_{ads}^2$, we can attribute an electrokinetic charge density σ_0^{PAMAM} to the places where dendrimers are adsorbed

$$\sigma_0^{PAMAM} = \frac{eZ_{eff}}{\pi a_{ads}^2} \tag{7}$$

Thus, we obtain the total electrokinetic charge density σ for a substrate with σ_0^{sub} with a given fractional surface coverage θ of PAMAM G10 dendrimers as follows:

$$\sigma = \sigma_0^{sub} + \theta\sigma_0^{PAMAM} \tag{8}$$

This equation considers the complete charge of the bare substrate rather than only the area that is not covered by dendrimers, which would correspond to 1-θ. Thereby, the charge compensation in between dendrimers and substrate in the adsorption sites is accounted for. A similar expression for linear superposition of charges has been postulated previously by Miklavic [91], Adamczyk and coworkers for streaming potential measurements of adsorbed linear as well as branched polyelectrolytes [38,45,46,92], and by Pericet-Camara et al. for direct force measurements with the colloidal probe technique [55]. Based on equations (7) and (8), we determined the effective charge for each fractional surface coverage on both substrates. The modified Grahame equation (3) was used to convert the measured ζ to σ while θ has been independently determined from the AFM images. Fig. 7b shows the thereby determined values for Z_{eff} as a function of the fractional surface coverage θ. The corresponding results obtained with the symmetric streaming potential cell are presented in the SI (cf. Fig. S13).

For both substrates, the dendrimeŕs effective charge was independent of the surface coverage. Hence, no inter-dendrimer charge regulation was present for the separation distances studied here. However, we found two very different effective charges for the two substrates. In the case of mica $Z_{eff}|_{\text{mica}} = 141 \pm 21$, which differs significantly from $Z_{eff}|_{\text{silica}} = 265 \pm 78$ on fused silica. The former value is much closer to the mean field approximation in a bulk solution of $Z_{eff} = 115$ under the conditions studied here, i.e., $I = 5$ mM. It should also be noted that all measurements were performed at pH 5. At this pH, the dendrimers should be nearly fully charged according to titration data [89]. However, it should be pointed out that this approximation is valid for low ionic strength [54]. This condition might not be strictly fulfilled for the ionic strength utilized here.

3.6. Effective charge as function of pH

To further elucidate the role of the substrate for the effective charge of the dendrimers, we varied the pH as a further parameter. The pH was varied only post-adsorption: The dendrimers were adsorbed first at pH 5, and then the pH of the solution was varied, while streaming potential data were acquired. The pH titrations were carried out in this way to ensure constant surface coverage. We assume that no dendrimers were removed during these measurements because it is known that dendrimers of higher generations, i.e., PAMAM > G6, adhere strongly to the substrate at all pH [90]. The corresponding ζ-values as function of the solution pH for the bare substrates have been presented previously in Fig. 3 for pH 4–10 and constant ionic strength $I = 5$ mM. For comparison, these data ($\theta = 0$) are also included in Fig. 8a and 8b, which show ζ for surface coverages of $\theta \approx 0.03$ (3 %) and $\theta \approx 0.09$ (9 %), respectively. Additionally, a higher surface coverage of $\theta \approx 0.13$ (13 %) was studied in the case of mica (cf. Fig. 8a).

For both dendrimer-covered substrates, a significant change of ζ as function of pH has been observed. A striking feature of both graphs is the

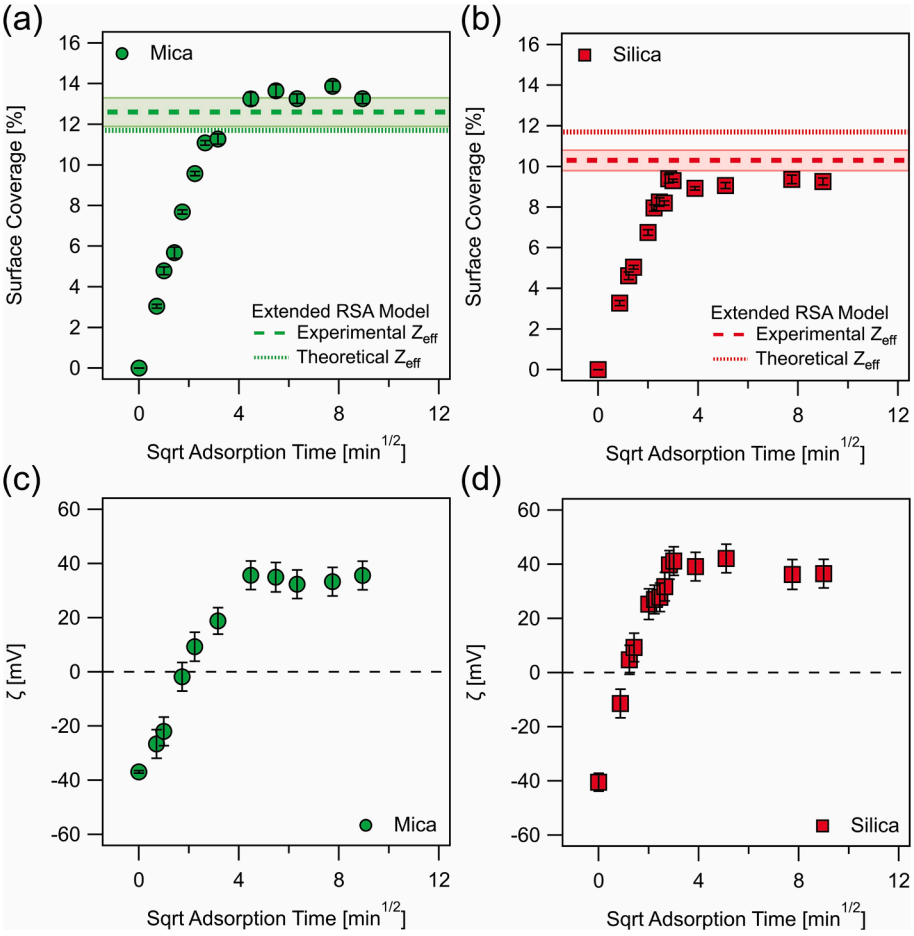

Fig. 6. Fractional surface coverage (a, b) and zeta-potential ζ (c, d) as functions of adsorption time $t^{1/2}$ at a constant pH 5 and ionic strength of 5 mM. The data for muscovite mica are shown in green (a, c), whereas the data for fused silica are shown in red (b, d). The dashed colored lines show the jamming limit calculated by experimental Z_{eff} from streaming potential (cf. Fig. 7b), while the dotted lines represent the jamming limit calculated by theoretical Z_{eff} (cf. Eq. (6)). The jamming limit was calculated as reported previously for PAMAM G10[28]. (For interpretation of the references to colour in this figure legend, the reader is referred to the web version of this article.)

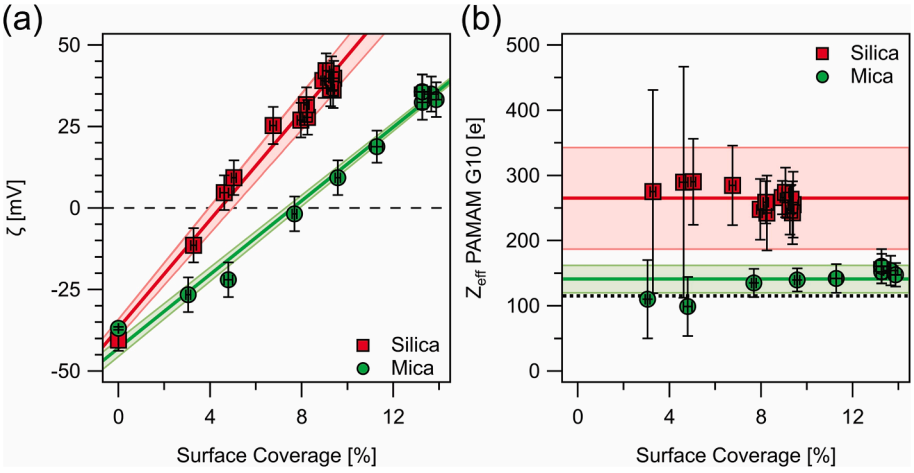

Fig. 7. (a) Zeta-potential ζ as a function of surface coverage for silica (red) and mica (green) at pH 5 and ionic strength $I = 5$ mM. The solid lines are fits assuming a linear dependence of ζ on the fractional surface coverage, including the fit errors as colored regions around the fit line. (b) Effective charge Z_{eff} in units of the elementary charge as a function of the surface coverage. The solid lines represent the mean of these Z_{eff} and the corresponding standard deviation (shaded area). The dotted line represents the mean field approximation for a PAMAM G10 dendrimer in solution according to equation (6). (For interpretation of the references to colour in this figure legend, the reader is referred to the web version of this article.)

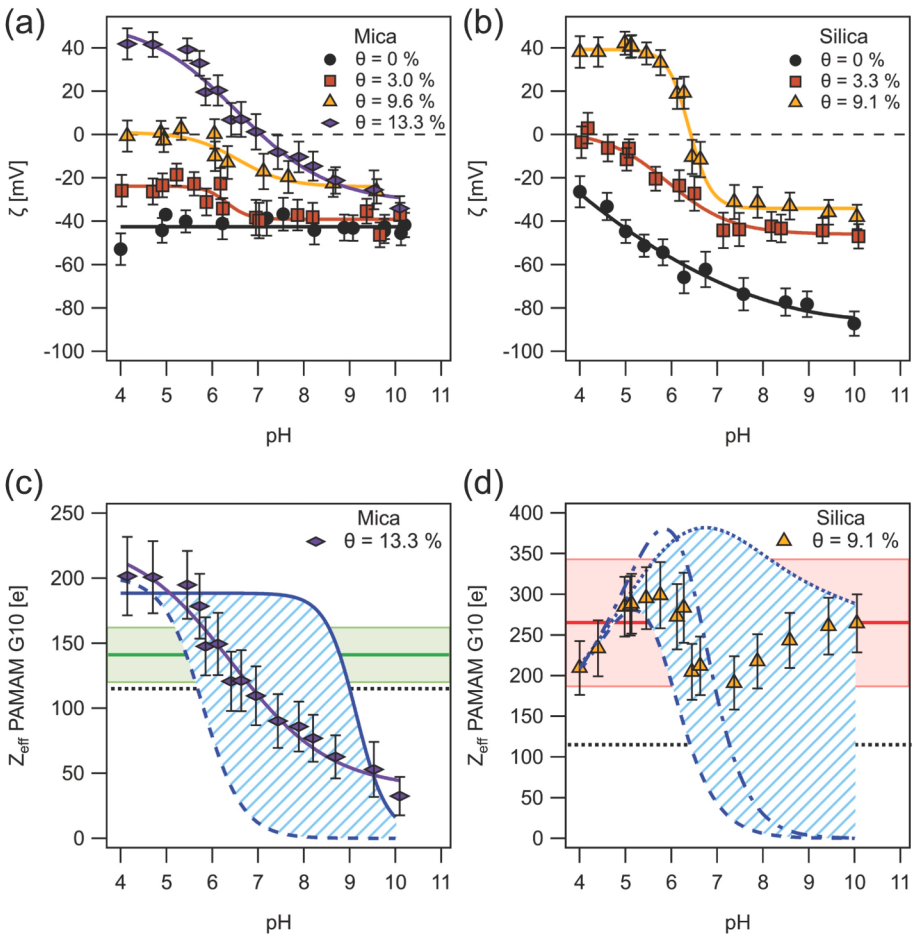

Fig. 8. (a) Zeta-potential ζ versus pH for bare mica (black) and three different surface coverages of PAMAM G10 dendrimers. (b) Zeta-potential ζ versus pH for fused silica (black) and two different surface coverages of PAMAM G10 dendrimers. (c) Calculated effective charge Z_{eff} of single PAMAM G10 dendrimers on mica as a function of pH. Z_{eff} was calculated only for the highest surface coverage. The dashed blue line represents ionization according to the Henderson-Hasselbalch equation with the pK = 5.8 [89] while the purple line represents a fit to a sigmoidal function, resulting in pK = 6.5 ± 0.1. The solid blue line represents the renormalized data from Michna et al. originating from the electrophoretic mobility of PAMAM G8 dendrimers [38]. The solid green line represents the mean experimental Z_{eff} on mica from Fig. 7b at pH 5 for comparison. (d) Calculated effective charge Z_{eff} of single PAMAM G10 dendrimers on silica as a function of pH. The dashed and broken blue lines represent the data for Z_{eff} calculated by Henderson-Hasselbalch with either the theoretical pK [89] or the pK obtained from the fit to the sigmoidal function in Fig. 8c (cf. purple line in Fig. 8c). The dotted blue line represents the sigmoidal fit to the experimental data for mica (cf. purple line in Fig. 8c) combined with Z_{eff} calculated by Eq. (6) for PAMAM at silica. In all cases, theoretical Z_{eff} were normalized following Eq. (9) and the variation in the effective inverse Debye-length κ_{eff} due to the pH dependence of the silica substrate was considered. For mica, a constant value (cf. black line Fig. 7a) was assumed. The solid red line represents the mean experimental Z_{eff} on silica (Fig. 7b) at pH 5. (For interpretation of the references to colour in this figure legend, the reader is referred to the web version of this article.)

presence of an isoelectric point where ζ and thus, the overall electrokinetic charge completely vanished and then changed sign with increasing pH. This charge-inversion effect only occurred at the highest surface coverages of $\theta = 0.13$ for mica and $\theta = 0.09$ for silica, respectively. Only for such high coverages a sufficient number of dendrimers adsorb and their positive charges allowed to compensate for the intrinsic charge of the collector substrates. A comparison of ζ as function of pH at the respective maximum coverage points is shown in Fig. S14. The overall pK for the PAMAM-covered substrates can be derived based on Ottewill's and Shaw's procedure [93]. However, for all coverages θ, a quasi-sigmoidal dependence of ζ on pH was observed for both substrates. The calculated pKs are roughly in line with the inflection points in Fig. 8a and 8b and are summarized in the supporting information (cf. Table S5).

The interpretation of the sigmoidal shape of ζ(pH) is more straightforward for mica than for silica, as former does not vary with pH. For mica, ζ of the bare surface remained constant for all the pH values studied here (cf. black data points in Fig. 8a). Hence, a constant σ can be assumed and any change in ζ(pH) must be attributed to the ionization of the adsorbed dendrimers as their coverage θ remained constant. Qualitatively, one expects that the tertiary amine groups are deprotonated in the acidic regime and thus the positive charge contributions diminish at higher pH, which has also been observed experimentally by bulk titrations [89]. Based on equations (7) and (8), we can calculate Z_{eff}(pH) from the ζ(pH)-measurements. The resulting data for Z_{eff}(pH) on mica and silica are shown in Fig. 8c and 8d for $\theta = 0.13$ and $\theta = 0.09$, respectively. The data for the lower surface coverages are shown in the SI (Fig. S15a and S15b) and show a similar pH dependence for mica. A fit according to a sigmoidal function gives a pK = 6.5 ± 0.1 for PAMAM G10 dendrimers on mica, which is in good correspondence with the extrapolation of pK = 5.8 by Cakara et al. for higher dendrimer generations G6-G10 in bulk solution [89]. The resulting dependence is shown as a dashed line according to the Henderson-Hasselbalch equation with $Z_{ref} \approx 200$ at pH = 4 and:

$$Z_{eff}(pH) = Z_{ref} \bullet \widetilde{Z}_{eff}(pH) = Z_{ref} \bullet e^{-(pK-pH)} \quad (9)$$

These data can also be compared to the electrophoretic mobility of single PAMAM G8 dendrimers in suspension as reported by Michna et al.

(cf. solid blue line in Fig. 8c) [38]. Please, notice that we normalized the experimental fit to the electrophoretic mobility data for PAMAM G8 dendrimers (cf. Fig. 2 in ref. [38]) to obtain $0 \leq \widetilde{Z}_{eff}(\mathrm{pH}) \leq 1$ and $\widetilde{Z}_{eff}(\mathrm{pH}=4)=1$ from the experimental data rather than the theoretical values according to Henderson-Hasselbalch. The experimental data for the PAMAM G8 dendrimers corroborate the limitations of Eq. (6), indicating the influence of the substrate on Z_{eff}.

For the PAMAM G10 dendrimers adsorbed on silica, Z_{eff}(pH) exhibited a more complex behavior. Silica varies its charge with pH as described within the framework of the 1-pK model with pK = 5.8 (cf. Fig. 2b) [75]. While the overall ζ(pH)-curves of the silica with adsorbed PAMAM G10 dendrimers showed a pronounced sigmoidal behavior (cf. Fig. 8b), the derived effective charge Z_{eff}(pH) of the single PAMAM dendrimers did not follow the same trend as on mica (cf. Fig. 8c). The effective charge for the PAMAM G10 dendrimers shows instead a slightly oscillatory behavior around a much higher effective charge of $Z_{eff} \sim 270$ and does not decline steeply in the basic regime as for PAMAM G10 dendrimers on mica or in bulk solution. This change is most likely attributed to the charging behavior of silica, which leads to an increased counterion concentration at the interface with increasing pH. Desorption of PAMAM G10 would be unlikely as origin for the oscillatory behavior of Z_{eff} and would occur only at very high pH if at all [38,90]. As a first approximation, we consider the influence of the substrate on the local ion concentration around the dendrimers *via* an effective inverse Debye length κ_{eff} [33]:

$$\kappa_{eff} = \kappa \cosh\left(\frac{e\psi_d}{k_B T}\right) \tag{10}$$

Here, κ is the inverse bulk Debye length of the electrolyte solution and ψ_d the diffuse layer potential at the solid substrate, which can be approximated by $\psi_d \simeq \zeta(\mathrm{pH})$. Please note that an expression analogous to Eq. (10) is used in the 3-body RSA model to account for the reduced interaction between dendrimers on a highly charged substrate [32,33]. By utilizing κ_{eff} at the interface rather than κ in Eq. (6) to calculate Z_{eff}, the influence of varying charge with pH on silica can be modeled. Here, we assume that the titration of the dendrimers and substrate are independent of each other and that the latter provides only modulation of the former by its diffuse layer. Hence, the results of Eq. (6) and Eq. (10) resulting in a $Z_{eff}(\mathrm{pH})$ due to counter-ion condensation are multiplied with $\widetilde{Z}_{eff}(\mathrm{pH})$ due to the deprotonation of the charged groups. Again, $\widetilde{Z}_{eff}(\mathrm{pH})$ results from the Henderson-Hasselbalch equation for dendrimer ionization (dashed blue line in Fig. 8c,d) or bulk electrophoretic mobility (solid blue line, Fig. 8c). The renormalized data from Michna et al. originating from the electrophoretic mobility of PAMAM G8 dendrimers was calculated analogously to the dotted blue line in Fig. 8d (cf. Fig. S16 in the SI). Interestingly, our data for the PAMAM G10 dendrimer Z_{eff} on silica corresponded rather well to the simple boundary conditions enforced in Fig. 8d. Noticeably, the decrease in Z_{eff} for $5.5 < \mathrm{pH} < 8$ is matched rather well. However, at higher pH values, when the dendrimer charge diminishes significantly, other processes, such as the direct charge regulation between the dendrimer and substrate [50,53], are playing an increasingly important role compared to counter ion condensation.

4. Conclusions

In this study, we found that the common assumption of the superposition of charge from the substrate and adsorbed polyelectrolytes (cf. Eq. (8)) holds with surprisingly good accuracy. We could also reproduce for mica the dependence of the streaming potential from PAMAM G10 dendrimer coverage as reported by Michna et al. for PAMAM G8 [38]. Hence, the ζ-potential indeed provides a good indicator for polyelectrolyte coverage as utilized in various studies, including for linear polyelectrolytes [44–46]. Moreover, the adsorption of charged biomacromolecules, such as humic acids, to membranes can be followed by streaming potential with high accuracy [94]. We did not find any indication of inter-dendrimer charge regulation. However, for fractional coverages of less than 20 %, the spacing between the dendrimers was larger than the Debye length, which is a typical length scale in which charge regulation plays a crucial role.

This study highlights the somehow neglected importance of substrates for the effective charge of macromolecules. As the effective charge governs the intermolecular interaction forces, they are crucial in the framework of the electrostatic RSA model. Our measurements clearly show that the commonly used approximation by Bocquet et al. [54] underestimates the effective charge in many cases, especially for highly charged substrates. In this case, the effective Debye length due to counterions from the substrates provides a much better approximation than the bulk Debye length. While this effect is not of importance for colloidal particles with diameters > 20 nm, it should be considered when describing the adsorption of macromolecules. The effective Debye length has been considered previously to model inter-molecular interaction potentials in the framework of the 3-body RSA model [33]. However, it is more consistent to include the effect of κ_{eff} also on the effective charge. Finally, there could also be an influence on direct force measurements. Previously, it has been assumed that Z_{eff} remains constant for heterogeneously charged surfaces [55]. However, for separation distances D between the two surfaces that are below the bulk Debye length, the counter ion concentration increases and might have an influence by a distance-dependent effect on κ_{eff} and thereby on Z_{eff}. For $D < \kappa^{-1}$ charge regulation also plays an important role, which is primarily of chemical origin [95,96]. Varying the electrolyte composition might help in the future to separate the mean-field approach to the effective charge by counter ion condensation from the influence of charge regulation, either between the adsorbed macromolecules themselves or between macromolecule and substrate.

CRediT authorship contribution statement

Matthias B. Engelhardt: Writing – review & editing, Writing – original draft, Visualization, Methodology, Investigation, Formal analysis, Conceptualization. **Paul Markus:** Writing – review & editing, Software, Methodology, Investigation, Formal analysis, Conceptualization. **Nicolas Helfricht:** Writing – review & editing, Methodology, Formal analysis. **Georg Papastavrou:** Writing – review & editing, Writing – original draft, Supervision, Resources, Project administration, Funding acquisition, Formal analysis, Conceptualization.

Declaration of competing interest

The authors declare that they have no known competing financial interests or personal relationships that could have appeared to influence the work reported in this paper.

Acknowledgments

G.P. thanks Dr. Brian Cahill (now Hochschule Bielefeld) for his help with early versions of the streaming potential setup. We thank Dr. Motoyoshi Kobayashi (University of Tsukuba, Japan) for access to the program for calculating the theoretical zeta-potential ζ. This study was funded by the Deutsche Forschungsgemeinschaft (DFG, German Research Foundation): 391977956-SFB 1357/B01, 491183248. M.B.E. thanks the Elite Network of Bavaria through the study program "Macromolecular Science".

Appendix A. Supplementary data

Supplementary data to this article can be found online at https://doi.org/10.1016/j.jcis.2025.02.008.

Data availability

Data will be made available on request.

References

[1] H. G. M. Van de Steeg, M. A. Cohen Stuart, A. De Keizer and B. H. Bijsterbosch, Langmuir, 8(10), 1992, 2538-2546. https://doi.org/10.1021/la00046a030.
[2] R.R. Netz, D. Andelman, Phys. Rep. 380 (1–2) (2003) 1–95, https://doi.org/10.1016/s0370-1573(03)00118-2.
[3] A.V. Dobrynin, M. Rubinstein, Prog. Polym. Sci. 30 (11) (2005) 1049–1118, https://doi.org/10.1016/j.progpolymsci.2005.07.006.
[4] Z. Adamczyk, Curr. Opin. Colloid Interface Sci. 17 (3) (2012) 173–186, https://doi.org/10.1016/j.cocis.2011.12.002.
[5] I. Szilagyi, G. Trefalt, A. Tiraferri, P. Maroni, M. Borkovec, Soft Matter 10 (15) (2014) 2479–2502, https://doi.org/10.1039/c3sm52132j.
[6] A. Abdurahman, K. Cui, J. Wu, S. Li, R. Gao, J. Dai, W. Liang, F. Zeng, Ecotox. Environ. Safe. 198 (2020) 110658, https://doi.org/10.1016/j.ecoenv.2020.110658.
[7] T. Hüffer, A. Praetorius, S. Wagner, F. Von der Kammer, T. Hofmann, Environ. Sci. Technol. 51 (5) (2017) 2499–2507, https://doi.org/10.1021/acs.est.6b04054.
[8] R.B. Schefer, A. Armanious, D.M. Mitrano, Environ. Sci. Technol. 57 (39) (2023) 14707–14716, https://doi.org/10.1021/acs.est.3c04180.
[9] J. Gregory, J. Colloid Interface Sci. 42 (2) (1973) 448–456, https://doi.org/10.1016/0021-9797(73)90311-1.
[10] P.M. Claesson, A. Dedinaite, O.J. Rojas, Adv. Colloid Interface Sci. 104 (1–3) (2003) 53–74, https://doi.org/10.1016/S0001-8686(03)00036-8.
[11] M. Schönhoff, J. Phys. Condens. Matter 15 (49) (2003) R1781, https://doi.org/10.1088/0953-8984/15/49/R01.
[12] M. Borkovec, I. Szilagyi, I. Popa, M. Finessi, P. Sinha, P. Maroni, G. Papastavrou, Adv. Colloid Interface Sci. 179 (2012) 85–98, https://doi.org/10.1016/j.cis.2012.06.005.
[13] J.N. Anker, W.P. Hall, O. Lyandres, N.C. Shah, J. Zhao, R.P. Van Duyne, Nat. Mater. 7 (2008) 442–453, https://doi.org/10.1038/nmat2162.
[14] J. Homola, Chem. Rev. 108 (2) (2008) 462–493, https://doi.org/10.1021/cr068107d.
[15] A. Michna, Adv. Colloid Interface Sci. 250 (2017) 95–131, https://doi.org/10.1016/j.cis.2017.09.004.
[16] D. Johannsmann, I. Reviakine, Nat. Rev. Methods Primers 4 (2024) 63, https://doi.org/10.1038/s43586-024-00340-4.
[17] H. Butt, K. Graf, M. Kappl, Physics and chemistry of interfaces, WILEY-VCH, Weinheim, 2003.
[18] R.R. Netz, J.-F. Joanny, Macromolecules 32 (26) (1999) 9013–9025, https://doi.org/10.1021/ma990263h.
[19] A.V. Dobrynin, A. Deshkovski, M. Rubinstein, PhysRevLett. 84 (14) (2000) 3101, https://doi.org/10.1103/PhysRevLett.84.3101.
[20] D.A. Tomalia, H. Baker, J. Dewald, M. Hall, G. Kallos, S. Martin, J. Roeck, J. Ryder, P. Smith, Macromolecules 19 (9) (1986) 2466–2468, https://doi.org/10.1021/ma00163a029.
[21] V.A. Kabanov, A.B. Zezin, V.B. Rogacheva, Z.G. Gulyaeva, M.F. Zansochova, J.G. H. Joosten, J. Brackman, Macromolecules 31 (15) (1998) 5142–5144, https://doi.org/10.1021/ma971643a.
[22] V.V. Tsukruk, Adv. Mater. 10 (3) (1998) 253–257, https://doi.org/10.1002/(SICI)1521-4095(199802)10:3<253::AID-ADMA253>3.0.CO;2-E.
[23] Z. Adamczyk, B. Siwek, M. Zembala, P. Belouschek, Adv. Colloid Interface Sci. 48 (1994) 151–280, https://doi.org/10.1016/0001-8686(94)80008-1.
[24] J. Feder, J. Theor. Biol. 87 (2) (1980) 237–254, https://doi.org/10.1016/0022-5193(80)90358-6.
[25] P. Kubala, P. Batys, J. Barbasz, P. Weroński, M. Cieśla, Adv. Colloid Interface Sci. 306 (2022) 102692, https://doi.org/10.1016/j.cis.2022.102692.
[26] P.R. Van Tassel, P. Viot, G. Tarjus, J. Chem. Phys. 106 (2) (1997) 761–770, https://doi.org/10.1063/1.473164.
[27] M. Morga, A. Michna, Z. Adamczyk, Colloid Surf. A 529 (2017) 302–310, https://doi.org/10.1016/j.colsurfa.2017.05.033.
[28] R. Pericet-Camara, G. Papastavrou, M. Borkovec, Langmuir 20 (8) (2004) 3264–3270, https://doi.org/10.1021/la035955k.
[29] J.W. Evans, RevModPhys. 65 (4) (1993) 1281, https://doi.org/10.1103/RevModPhys.65.1281.
[30] J. Talbot, G. Tarjus, P.R. Van Tassel, P. Viot, Colloid Surf. A 165 (1–3) (2000) 287–324, https://doi.org/10.1016/S0927-7757(99)00409-4.
[31] Z. Adamczyk, P. Warszyński, Adv. Colloid Interface Sci. 63 (1996) 41–149, https://doi.org/10.1016/0001-8686(95)00281-2.
[32] R. Pericet-Camara, B.P. Cahill, G. Papastavrou, M. Borkovec, Chem. Commun. 3 (2007) 266–268, https://doi.org/10.1039/b612249c.
[33] B.P. Cahill, G. Papastavrou, G.J. Koper, M. Borkovec, Langmuir 24 (2) (2008) 465–473, https://doi.org/10.1021/la7021352.
[34] A.V. Delgado, F. González-Caballero, R.J. Hunter, L.K. Koopal, J. Lyklema, J. Colloid Interface Sci. 309 (2) (2007) 194–224, https://doi.org/10.1016/j.jcis.2006.12.075.
[35] R.J. Hunter, Zeta potential in colloid science, Elsevier, 1981.
[36] R.W. O'Brien, L.R. White, J. Chem. Soc., Faraday Trans. 2 (74) (1978) 1607–1626, https://doi.org/10.1039/F29787401607.
[37] H. Ohshima, J. Colloid Interface Sci. 163 (2) (1994) 474–483, https://doi.org/10.1006/jcis.1994.1126.
[38] A. Michna, Z. Adamczyk, K. Sofińska, K. Matusik, J. Colloid Interface Sci. 485 (2017) 232–241, https://doi.org/10.1016/j.jcis.2016.09.007.
[39] R. Zimmermann, W. Norde, M.A. Cohen Stuart, C. Werner, Langmuir 21 (11) (2005) 5108–5114, https://doi.org/10.1021/la050191p.
[40] Z. Adamczyk, K. Sadlej, E. Wajnryb, M. Nattich, M.L. Ekiel-Jeżewska, J. Bławdziewicz, Adv. Colloid Interface Sci. 153 (1–2) (2010) 1–29, https://doi.org/10.1016/j.cis.2009.09.004.
[41] Z. Adamczyk, M. Zaucha, M. Zembala, Langmuir 26 (12) (2010) 9368–9377, https://doi.org/10.1021/la1003534.
[42] C. V. Ruiz M, M. Terlinden, M. Engelhardt, G. Magnabosco, G. Papastavrou, N. Vogel, M. Thommes and J. Bachmann, Adv. Mater. Interfaces, 10(33), 2023, 2300436. https://doi.org/10.1002/admi.202300436.
[43] A. Hofer, N. Taccardi, M. Moritz, C. Wichmann, S. Hübner, D. Drobek, M. Engelhardt, G. Papastavrou, E. Spiecker, C. Papp, RSC Adv. 13 (6) (2023) 4011–4018, https://doi.org/10.1039/D2RA07585G.
[44] A. Michna, Z. Adamczyk, K. Kubiak, K. Jamroży, J. Colloid Interface Sci. 428 (2014) 170–177, https://doi.org/10.1016/j.jcis.2014.04.013.
[45] M. Morga, Z. Adamczyk, J. Colloid Interface Sci. 407 (2013) 196–204, https://doi.org/10.1016/j.jcis.2013.05.069.
[46] M. Morga, Z. Adamczyk, S. Gödrich, M. Oćwieja, G. Papastavrou, J. Colloid Interface Sci. 456 (2015) 116–124, https://doi.org/10.1016/j.jcis.2015.05.044.
[47] B. Jachimska, K. Tokarczyk, J. Phys. Chem. C 120 (35) (2016) 19678–19685, https://doi.org/10.1021/acs.jpcc.6b05020.
[48] A. Michna, A. Pomorska, M. Nattich-Rak, M. Wasilewska, Z. Adamczyk, J. Phys. Chem. C 124 (32) (2020) 17684–17695, https://doi.org/10.1021/acs.jpcc.0c04638.
[49] L. Muresan, P. Maroni, I. Popa, M. Porus, R. Longtin, G. Papastavrou, M. Borkovec, Macromolecules 44 (13) (2011) 5069–5071, https://doi.org/10.1021/ma201103n.
[50] M. Porus, F. Clerc, P. Maroni, M. Borkovec, Macromolecules 45 (9) (2012) 3919–3927, https://doi.org/10.1021/ma3004295.
[51] M. Gosika, P.K. Maiti, Soft Matter 14 (10) (2018) 1925–1938, https://doi.org/10.1039/C8SM00179K.
[52] P. Wolski, T. Panczyk, J. Phys. Chem. C 123 (36) (2019) 22603–22613, https://doi.org/10.1021/acs.jpcc.9b05752.
[53] M. Gosika, T. Mandal, P.K. Maiti, Langmuir 36 (20) (2020) 5492–5501, https://doi.org/10.1021/acs.langmuir.0c00208.
[54] L. Bocquet, E. Trizac, M. Aubouy, J. Chem. Phys. 117 (17) (2002) 8138–8152, https://doi.org/10.1063/1.1511507.
[55] R. Pericet-Camara, G. Papastavrou, M. Borkovec, Macromolecules 42 (5) (2009) 1749–1758, https://doi.org/10.1021/ma802374z.
[56] W. de Poel, S. Pintea, J. Drnec, F. Carla, R. Felici, P. Mulder, J.A.A.W. Elemans, W. J.P. van Enckevort, A.E. Rowan, E. Vlieg, Surf. Sci. 619 (2014) 19–24, https://doi.org/10.1016/j.susc.2013.10.008.
[57] W. Kern and D. A. Puotinen, RCA Review, 31(2), 1970, 187-206, A1970H070100002.
[58] S.L. Walker, S. Bhattacharjee, E.M.V. Hoek, M. Elimelech, Langmuir 18 (6) (2002) 2193–2198, https://doi.org/10.1021/la011284j.
[59] J. Schindelin, I. Arganda-Carreras, E. Frise, V. Kaynig, M. Longair, T. Pietzsch, S. Preibisch, C. Rueden, S. Saalfeld, B. Schmid, J.Y. Tinevez, D.J. White, V. Hartenstein, K. Eliceiri, P. Tomancak, A. Cardona, Nat. Methods 9 (7) (2012) 676–682, https://doi.org/10.1038/nmeth.2019.
[60] R.A. Van Wagenen, J. Colloid Interface Sci. 76 (2) (1980) 305–314, https://doi.org/10.1016/0021-9797(80)90374-4.
[61] C. Werner, H. Körber, R. Zimmermann, S. Dukhin, H.J. Jacobasch, J. Colloid Interface Sci. 208 (1) (1998) 329–346, https://doi.org/10.1006/jcis.1998.5787.
[62] M. Zembala, Z. Adamczyk, P. Warszyński, Colloid Surf. A 222 (1–3) (2003) 329–339, https://doi.org/10.1016/s0927-7757(03)00253-x.
[63] M. Zembala, Adv. Colloid Interface Sci. 112 (1–3) (2004) 59–92, https://doi.org/10.1016/j.cis.2004.08.001.
[64] K.S. Spiegler, Desalination 15 (1) (1974) 135–140, https://doi.org/10.1016/S0011-9164(00)82067-6.
[65] M.C. Wilbert, S. Delagah, J. Pellegrino, J. Membr. Sci. 161 (1–2) (1999) 247–261, https://doi.org/10.1016/S0376-7388(99)00117-9.
[66] H. Ohshima, Theory of colloid and interfacial electric phenomena, Academic Press, 2006.
[67] P.J. Scales, F. Grieser, T.W. Healy, Langmuir 6 (3) (1990) 582–589, https://doi.org/10.1021/la00093a012.
[68] K. Fa, V.K. Paruchuri, S.C. Brown, B.M. Moudgil, J.D. Miller, Phys. Chem. Chem. Phys. 7 (2005) 678–684, https://doi.org/10.1039/b417902a.
[69] M. Herzberg, S. Dobberschütz, D. Okhrimenko, N.E. Bovet, M.P. Andersson, S.L. S. Stipp, T. Hassenkam, EPL 130 (3) (2020) 36001, https://doi.org/10.1209/0295-5075/130/36001.
[70] C.E. Marshall, L.L. McDowell, Soil Sci. 99 (2) (1965) 115–131, https://doi.org/10.1097/00010694-196502000-00009.
[71] U. Raviv, P. Laurat, J. Klein, J. Chem. Phys. 116 (12) (2002) 5167–5172, https://doi.org/10.1063/1.1447911.
[72] P.J. Sides, D. Faruqui, A.J. Gellman, Langmuir 25 (3) (2009) 1475–1481, https://doi.org/10.1021/la802752g.
[73] M. Kobayashi, M. Skarba, P. Galletto, D. Cakara, M. Borkovec, J. Colloid Interface Sci. 292 (1) (2005) 139–147, https://doi.org/10.1016/j.jcis.2005.05.093.
[74] J.S. Lyons, D.N. Furlong, T.W. Healy, Aust. J. Chem. 34 (6) (1981) 1177–1187, https://doi.org/10.1071/ch9811177.
[75] P.J. Scales, F. Grieser, T.W. Healy, L.R. White, D.Y.C. Chan, Langmuir 8 (3) (1992) 965–974, https://doi.org/10.1021/la00039a037.

[76] T. Hiemstra, W.H. Van Riemsdijk, G.H. Bolt, J. Colloid Interface Sci. 133 (1) (1989) 91–104, https://doi.org/10.1016/0021-9797(89)90284-1.
[77] T. Hiemstra, J.C.M. De Wit, W.H. Van Riemsdijk, J. Colloid Interface Sci. 133 (1) (1989) 105–117, https://doi.org/10.1016/0021-9797(89)90285-3.
[78] S.H. Behrens, D.I. Christl, R. Emmerzael, P. Schurtenberger, M. Borkovec, Langmuir 16 (6) (2000) 2566–2575, https://doi.org/10.1021/la991154z.
[79] M. Kobayashi, F. Juillerat, P. Galletto, P. Bowen, M. Borkovec, Langmuir 21 (13) (2005) 5761–5769, https://doi.org/10.1021/la046829z.
[80] D. Kosior, M. Morga, P. Maroni, M. Cieśla, Z. Adamczyk, J. Phys. Chem. C 124 (8) (2020) 4571–4581, https://doi.org/10.1021/acs.jpcc.9b10870.
[81] A.R. Crothers, C. Li, C.J. Radke, Adv. Colloid Interface Sci. 288 (2021) 102335, https://doi.org/10.1016/j.cis.2020.102335.
[82] M. Zembala, Z. Adamczyk, Langmuir 16 (4) (2000) 1593–1601, https://doi.org/10.1021/la9905970.
[83] J. N. Israelachvili, G. E. Adams, J. Chem. Soc., Faraday Trans. 1 (74) (975-1001) 1978. https://doi.org/10.1039/f19787400975.
[84] D.A. Tomalia, Mater. Today 8 (3) (2005) 34–46, https://doi.org/10.1016/S1369-7021(05)00746-7.
[85] T.A. Betley, M.M. Banaszak Holl, B.G. Orr, D.R. Swanson, D.A. Tomalia, J.R. Baker, Langmuir 17 (9) (2001) 2768–2773, https://doi.org/10.1021/la001297h.
[86] V.N. Bliznyuk, F. Rinderspacher, V.V. Tsukruk, Polymer 39 (21) (1998) 5249–5252, https://doi.org/10.1016/S0032-3861(98)00069-X.
[87] A. Hierlemann, J.K. Campbell, L.A. Baker, R.M. Crooks, A.J. Ricco, J. Am. Chem. Soc. 120 (21) (1998) 5323–5324, https://doi.org/10.1021/ja974283f.
[88] J. Li, L.T. Piehler, D. Qin, J.R. Baker, D.A. Tomalia, D.J. Meier, Langmuir 16 (13) (2000) 5613–5616, https://doi.org/10.1021/la000035c.
[89] D. Cakara, J. Kleimann, M. Borkovec, Macromolecules 36 (11) (2003) 4201–4207, https://doi.org/10.1021/ma0300241.
[90] R. Longtin, P. Maroni, M. Borkovec, Langmuir 25 (5) (2009) 2928–2934, https://doi.org/10.1021/la8038818.
[91] S.J. Miklavic, J. Colloid Interface Sci. 171 (2) (1995) 446–455, https://doi.org/10.1006/jcis.1995.1201.
[92] M. Dabkowska, Z. Adamczyk, J. Colloid Interface Sci. 366 (1) (2012) 105–113, https://doi.org/10.1016/j.jcis.2011.09.030.
[93] R.H. Ottewill, J.N. Shaw, Kolloid z. z. Polym. 218 (1) (1967) 34–40, https://doi.org/10.1007/bf01517273.
[94] A.E. Childress, M. Elimelech, J. Membr. Sci. 119 (2) (1996) 253–268, https://doi.org/10.1016/0376-7388(96)00127-5.
[95] S.L. Carnie, D.Y.C. Chan, J. Colloid Interface Sci. 161 (1) (1993) 260–264, https://doi.org/10.1006/jcis.1993.1464.
[96] G. Trefalt, S.H. Behrens, M. Borkovec, Langmuir 32 (2) (2016) 380–400, https://doi.org/10.1021/acs.langmuir.5b03611.